Title

INVESTIGATION OF BIOGEOPHYSICAL FEEDBACK ON THE AFRICAN CLIMATE USING A 2-DIMENSIONAL MODEL

Journal

JOURNAL OF CLIMATE, 3(3)

ISSN

0894-8755

Authors

XUE, YK
LIOU, KN
KASAHARA, A

Publication Date

1990-03-01

DOI

10.1175/1520-0442(1990)003<0337:IOBFOT>2.0.CO;2

Peer reviewed

Investigation of Biogeophysical Feedback on the African Climate Using a Two-Dimensional Model

YONGKANG XUE* AND KUO-NAN LIOU

Department of Meteorology, University of Utah, Salt Lake City, Utah

AKIRA KASAHARA

*National Center for Atmospheric Research,** Boulder, Colorado*

(Manuscript received 24 January 1989, in final form 9 November 1989)

ABSTRACT

A 2-D zonally averaged, time-dependent climate model has been developed to study the biogeophysical feedback for the climate of Africa. A numerical scheme has been specifically designed for the model to ensure the conservation of mass, momentum, energy, and water vapor. A control experiment has been carried out in which the solar zenith angle was varied from 15 June to 30 July. The simulated results are presented using averages over the last 30 days. The simulated temperature, humidity, and winds for July mean conditions compare reasonably well with zonally averaged, observed values.

A vegetation layer has been incorporated in the present 2-D climate model. Using the coupled climate–vegetation model, we performed two tests involving the removal and expansion of the Sahara Desert. Results show that variations in the surface conditions produce a significant feedback to the climate system. The feedback from the land surface to the atmosphere affects not only precipitation and cloud cover, but also temperature, radiation budgets, and wind fields. The simulation responses to the temperature and zonal wind in the case of an expanded desert agree with the climatological data for African dry years.

Perturbed simulations have also been performed by changing the albedo only, without allowing the variation in the vegetation layer. In this case, the model is unable to reproduce the observed temperature, humidity, and wind fields over the African continent for both dry and wet years. We show that the variation in latent heat release is significant and is related to changes in the vegetation cover in a number of ways. As the desert is expanded, the decrease in latent heat is much larger than the increase in sensible heat generated by the hot surface. The specific humidity in the atmosphere decreases due to less evaporation from the ground and a reduction in the horizontal convergence of water vapor transport. As a result, precipitation and cloud cover are reduced.

1. Introduction

During the 1970s and 1980s, drought and famine extended throughout the Sahel region at the edge of the Sahara. It has been suggested that desertification through overgrazing or excessive cultivation of marginal land played an important role in the African drought. To study how such disasters are created, significant research has been undertaken to investigate the feedback of tropical desertification on regional and global climate.

Deserts can be produced by the following factors: 1) the separation of the region from an oceanic moisture source by distance or topography, as in the Mongolian Gobi Desert; 2) an association with descending branches of the tropical Hadley circulation, as in most subtropical deserts; and 3) denudation caused by overgrazing. With respect to factor 3), there appears to be no scientific consensus at this time regarding the mechanisms and responses of the climate system that trigger desertification.

In his pioneering study, Charney (1975) proposed a biogeophysical feedback mechanism for the creation and perpetuation of deserts and droughts. He studied the feedback relationship between sinking motion and the albedo effect using a 2-D model. He indicated that desert areas reflect more solar radiation to space and form a radiative heat sink. Because the surface stores little heat, the air loses heat, descends, and compresses adiabatically. This sinking motion suppresses rainfall in desert areas. Furthermore, Charney et al. (1975) used a general circulation model (GCM) to investigate

* Present affiliation: Department of Meteorology, University of Maryland, College Park, MD 20742.

** The National Center for Atmospheric Research is sponsored by the National Science Foundation.

Corresponding author address: Professor Kuo-Nan Liou, Department of Meteorology, The University of Utah, 819 William C. Browning Building, Salt Lake City, UT 84112.

the importance of the effects of surface albedo on precipitation in the Sahara Desert regions during summer. They showed that the precipitation in the high-albedo experiment was substantially smaller than that in the low-albedo experiment. Similar sensitivity tests were also performed by Potter et al. (1975) and Elsaesser et al. (1976) using a 2-D zonally averaged model. Their results were similar in that precipitation was lower in the high-albedo zone.

The surface temperature is warmer in the desert than over the vegetated surface. In Charney's experiments, however, the temperature actually decreased after the albedo was increased. Ripley (1976) pointed out that Charney et al. (1975) ignored evapotranspiration due to vegetation. Less evaporation would lead to higher surface temperatures over the desert areas. Later, Charney et al. (1977) included a simple parameterization of the evaporation rate in a GCM to study the albedo feedback. The soil moisture was kept constant in the experiment. The results revealed that changes in the evaporation rate are as important as changes in the albedo. Although the rainfall still decreased with increased albedo, the effects of the albedo change were found to be more complicated than originally postulated by Charney (1975).

Because the soil moisture content affects atmospheric conditions by influencing not only the albedo of bare soil, but also the evaporation and hence the energy balance at the surface, there is an increasing awareness of the role that surface hydrology may play in the evolution of climate. Walker and Rowntree (1977) investigated the effects of soil moisture on precipitation patterns. The albedo was fixed in the experiments. Their results show that rainfall is strongly influenced by the dryness of the underlying surface. Below 500 mb, temperatures in dry soil cases were higher than in wet soil cases. This differs from the experiments with albedo change only, in which the atmosphere is cooled by albedo increases.

Sud and Fennessy (1982) used a simple soil moisture equation in a GCM to study the influence of surface albedo on the July circulation in semiarid regions and the energy balance at the ground. Shukla and Mintz (1982) performed model experiments involving the introduction of wet and dry soil in the initial soil moisture content. They found that the soil moisture condition noticeably affected large-scale synoptic patterns. In view of the above, it is necessary to combine the roles of increased surface albedo and reduced soil moisture simultaneously in order to study the interactions and feedbacks of surface processes to the thermodynamic behavior of the atmosphere.

Hansen et al. (1983) incorporated a two-layer soil moisture model in a GCM. This soil moisture model was later used by Rind (1982, 1984) to study the influence of surface characteristics on the hydrological cycle. Laval and Picon (1986) studied the effects of changes in the Sahel surface albedo. In their experiments, both albedo and soil moisture were allowed to change. The results suggested that variations in albedo can induce changes in the zonal circulation, but they did not include vegetation effects in the model and sensitivity experiments. In a GCM simulation, Sud et al. (1988) found that reduced surface roughness does not produce significant changes in either the surface evaporation or sensible heat; however, it reduces the surface stress and produces variations in the convergence of horizontal water vapor transport.

Although the effects of albedo and soil moisture on precipitation, mean meridional circulation, and sea level pressure have been widely investigated, there are significant variations in the simulation results. As an example, there are different numerical results regarding the impact of surface desertification on temperature changes. These results indicate the need to evaluate carefully the manner in which the surface condition is incorporated in climate models. A more realistic modeling of land evapotranspiration is needed.

Dickinson et al. (1981), Dickinson (1984), and Dickinson et al. (1986) coupled a vegetation canopy model with a two-layer moisture model. A comprehensive boundary layer package that is termed the Biosphere–Atmosphere Transfer Scheme (BATS) has been developed for incorporation in the NCAR GCM. It contains parameterizations of heat and moisture transport in the vegetation canopy, surface, and rooting zone soil layer. Using this model, the effect of deforestation in the Amazon Basin was studied by Dickinson and Henderson-Sellers (1988). The deforestation experiment shows that surface pressure decreases, temperature increases, vertical ascent is weakened, and, at the same time, seasonal mean precipitation changes insignificantly. More recently, a biosphere model has been developed by Sellers et al. (1986) to calculate the transfer of energy, mass, and momentum between the atmosphere and the vegetated surface.

To study the interactions between the surface and atmospheric processes, not only is a suitable atmospheric model required, but also an adequate boundary layer, as has been discussed previously. A proper evaluation of the surface feedback to climate can be made only when all comparable components of the energy balance are considered, including albedo and soil moisture variations. The objective of this paper is to investigate the biogeophysical feedback on the African climate using a combined atmospheric and surface hydrological model. Because the climate pattern in Africa is fairly zonally symmetric, as reported by Flohn (1972), we have developed a 2-D climate model in the present study. The 2-D model has the advantage of computational economy and, at the same time, many atmospheric processes may be explicitly included in the model. In connection with the 2-D climate model, we have incorporated two soil layers and one vegetation layer to evaluate the transport of sensible and latent heat from the ground. Based on the scheme proposed

by Dickinson et al. (1986), a vegetation model has also been developed in this study. Using the present comprehensive surface model, we investigate the physical feedback of the change in surface characteristics to the cloud cover, precipitation, evaporation, circulation, radiation budget, temperature, and other climate factors in Africa.

In section 2, a brief description of the present model and physical parameterizations is presented. In section 3 the designed experiments, data sources, and results of the model simulations are described. Conclusions are given in section 4.

2. The 2-D zonally averaged climate model

a. The model

The present 2-D model is a 19-layer, zonally averaged climate model. The model uses a spherical coordinate system horizontally and a pressure-coordinate system vertically. The governing equations are the conservation of mass, energy, water vapor, and two components of momentum. These are:

$$\frac{\partial u}{\partial t}+\frac{\partial(uv\mu)}{\partial y}+\frac{\partial(u\omega)}{\partial p}-f'v=g\frac{\partial \tau_u}{\partial p}+F_u, \quad (1)$$

$$\frac{\partial v}{\partial t}+\frac{\partial(vv\mu)}{\partial y}+\frac{\partial(v\omega)}{\partial p}+f'u=g\frac{\partial \tau_v}{\partial p}+F_V-g\frac{\partial z}{a\partial\phi}, \quad (2)$$

$$\frac{\partial T}{\partial t}+\frac{\partial(Tv\mu)}{\partial y}+\frac{\partial(T\omega)}{\partial p}-\frac{RT\omega}{C_p p}=\frac{Q+Q_r}{C_p}+g\frac{\partial \tau_T}{\partial p}+F_T, \quad (3)$$

$$\frac{\partial q}{\partial t}+\frac{\partial(qv\mu)}{\partial y}+\frac{\partial(q\omega)}{\partial p}=-\frac{Q}{L}+g\frac{\partial \tau_q}{\partial p}+F_q, \quad (4)$$

$$\frac{\partial(v\mu)}{\partial y}+\frac{\partial\omega}{\partial p}=0, \quad (5)$$

$$g\frac{\partial z}{\partial p}+\frac{RT}{p}=0, \quad (6)$$

where t is the time, T the temperature, u and v the wind velocity components in λ and ϕ directions, respectively, q the specific humidity, ω the vertical velocity in the pressure coordinate, $\mu=\cos\phi$, $y=a\sin\phi$, a the radius of the earth, $f'=f+u\tan\phi/a$, f the Coriolis parameter, g the gravitational constant, C_p the specific heat at constant pressure, L the latent heat of condensation, and Q_r and Q the radiation and condensation heating rates, respectively. Also, the vertical eddy flux and horizontal diffusion terms have been denoted by τ_x and F_x, respectively, where the subscript x can be u, v, T, or q.

The boundary conditions at the top of the atmosphere are that the vertical velocity and vertical fluxes vanish. To conserve mass and horizontal fluxes in the y-direction for the 2-D model, the lateral boundary conditions are $v=0$, and $\partial x/\partial y=0$, where x may be μu, μv, T, or ω. These boundary conditions imply that $\omega=0$ and the surface pressure p_s is constant at the lateral boundary. The horizontal diffusion components F_u, F_T, and F_q are also set to zero.

The vertical eddy fluxes for momentum, temperature, and specific humidity may be parameterized in the forms

$$\tau_u=-\rho K_m\frac{\partial u}{\partial z}, \quad (7)$$

$$\tau_v=-\rho K_m\frac{\partial v}{\partial z}, \quad (8)$$

$$\tau_T=-\rho K_T\left(\frac{1000}{P}\right)^{R/C_p}\left(\frac{\partial\theta}{\partial z}-\gamma_c\right), \quad (9)$$

$$\tau_q=-\rho K_q\frac{\partial q}{\partial z}, \quad (10)$$

where K_m denotes the eddy viscosity, K_T the eddy thermal diffusion coefficient, K_q the eddy water vapor diffusion coefficient, ρ the air density, R the gas constant for air, γ_c the countergradient lapse rate (Deardorff 1972), θ the potential temperature. Following Oliger et al. (1970), we set $K_m=K_q=K_T=K$ in the model, where K is a function of $(\partial\theta/\partial z-\gamma_c)$. The parameterization of the horizontal diffusion for momentum, temperature, and humidity has been extensively investigated in the past. In the present study we follow the methodology described by Holloway and Manabe (1970) and Oliger et al. (1970) for the diffusion terms in spherical coordinates.

b. Parameterization of convection and precipitation

In the model, superadiabatic lapse rates may occur and lead to instability. We apply convective adjustment with an additional constraint that the heat content of the adjacent two layers is conserved, i.e.,

$$\sum_{i=1}^{2}\rho_i T_i\Delta z_i=\text{const.} \quad (11)$$

The convective adjustment routine examines a vertical column of grid points, starting at the bottom of the model and progressing successively toward the top of the atmosphere. For a saturated layer, the excess water vapor is rained out as precipitation and, at the same time, latent heat is added to the layer. The process is controlled by the constraint that

$$C_p\frac{dT}{dt}=-L\frac{dq}{dt}. \quad (12)$$

Because the saturation specific humidity q_s varies according to temperature, the adjusted value is given by

$$q' = q_s + \frac{dq_s}{dT}\delta T. \tag{13}$$

From Eq. (12), we may write $C_p\delta T = L(q - q')$ where q is the original specific humidity. Using Eq. (13) to eliminate δT, we obtain

$$q' = \left(q_s + \frac{L}{C_p}\frac{dq_s}{dT}q\right)\Big/\left(1 + \frac{L}{C_p}\frac{dq_s}{dT}\right). \tag{14}$$

The precipitation in units of mass per area in the ith model layer may then be computed from

$$P_i = \rho_i(q_i - q_i')\Delta z_i. \tag{15}$$

The total precipitation is then the sum of all individual layer precipitation.

c. Parameterization of radiation and cloud processes

The radiation package developed by Liou and Ou (1981, 1983) is used in the present model. To form clouds in connection with radiation calculations, we use the scheme proposed by Geleyn (1981). When the predicted relative humidity h is greater than a prescribed value, it is assumed that a water and/or ice cloud may be formed. The cloud cover c in this case is computed from an empirical equation. If h is smaller than or equal to the prescribed value h_c, however, no cloud is allowed to form. Thus,

$$c = \begin{cases} g(h), & h > h_c \\ 0, & h \leqslant h_c, \end{cases} \tag{16}$$

where the empirical equation is given by

$$g(h) = \{[h - h_c(\sigma)]/[1 - h_c(\sigma)]\}^2. \tag{17}$$

The critical relative humidity h_c is a function of σ and has the form

$$h_c = 1 - 2\sigma(1 - \sigma)[1 + 1.732(\sigma - 0.05)], \tag{18}$$

where $\sigma = p/p_s$, with p_s the surface pressure.

In the present model, clouds are allowed to form in all layers except the lowest layer. When fractional cloud covers are computed, they are assumed to fill the entire vertical layer. For radiative transfer calculations, we perform a cloud compaction, according to the scheme proposed by Liou et al. (1985), to obtain high, middle, and low cloud types. These model clouds are defined, respectively, in the pressure ranges $p < 600$ mb, $600 < p < 800$ mb, and $p > 800$ mb. The total cloud cover is computed from a scheme that assumes random overlap.

d. Modeling of soil and vegetation layers

The vegetation layer in the present model is represented by a single vertical grid point, which includes a foliage temperature. Moreover, a two-layer soil model is coupled with the vegetation canopy model. The foliage in the model is assumed to have zero heat capacity. The exchanges of moisture and energy among the vegetation, soil, and air are calculated interactively. The parameterization of the vegetation layer and notations used in the present model basically follow those proposed by Dickinson and his associates cited previously and by Deardorff (1978); however, a number of modifications, refinements, and simplifications in connection with the present model were made.

The prediction equations for the total soil water content in the rooting zone, S_{tw}, and the surface water content, S_{sw}, may be derived, based on the conservation principle for water, in the forms

$$\frac{\partial S_{sw}}{\partial t} = P(1 - \sigma_f) - R_s + TR - bE_{tr} - E_g + D_w, \tag{19}$$

$$\frac{\partial S_{tw}}{\partial t} = P(1 - \sigma_f) - R_s - R_g - E_{tr} - E_g + D_w, \tag{20}$$

where P denotes the precipitation, σ_f the vegetation cover, R_s the surface runoff, E_{tr} transpiration, E_g evaporation from the surface, and D_w the excess water dripping from leaves, which is computed from $W_f - W_{f\max}$, with W_f the water storage and $W_{f\max}$ a prescribed maximum value. Also in these equations, R_g is the leakage down to the subsoil, b the fraction of water that plants absorb at the upper soil layer, which is the ratio of the roots in the upper layer to those in the total column, and TR the downgradient rate of water transfer from the lower soil layer to the surface layer. The complete hydrological cycle near the ground has been accounted for in these two equations.

The water storage on foliage per unit land surface area is denoted by W_f. Its time rate of change may be obtained from the following prediction equation:

$$\frac{\partial W_f}{\partial t} = \sigma_f P - E_f + E_{tr}, \tag{21}$$

where E_f denotes evaporation from the foliage.

Following Deardorff (1978), the "force-restore" method has been used to calculate the ground temperature T_{g1} and the subsurface temperature T_{g2}. The prediction equations may be expressed by

$$\frac{\partial T_{g1}}{\partial t} = c_1\frac{h_s}{\rho_s c_s d_1} - c_2\frac{T_{g1} - T_{g2}}{\tau_1}, \tag{22}$$

$$\frac{\partial T_{g2}}{\partial t} = \frac{h_s}{\rho_s c_s d_2}, \tag{23}$$

where c_1, c_2, and τ_1 are certain constants, d_1 the soil depth influenced by a periodic heating rate, d_2 the exponential folding depth of the annual temperature wave, $\rho_s c_s$ the specific heat of the subsurface layer per unit mass, and h_s the forcing term, which may be obtained from the surface heat budget. The detailed pa-

rameterizations for the terms in the preceding equations can be found in Xue (1988).

The most important physical quantities through which a vegetation layer affects the atmosphere are the sensible and latent heat transport from the covered surface. The vertical flux of water vapor from the canopy τ_{qs} and the heat flux to the atmosphere from the vegetation layer τ_{Ts} may be expressed by

$$\tau_{qs} = \rho_a C_D |\vec{v}|_a (q_{af} - q_a), \tag{24}$$

$$\tau_{Ts} = \rho_a C_D |\vec{v}|_a (T_{af} - T_a), \tag{25}$$

where C_D denotes the drag coefficient, ρ_a the air density, $|\vec{v}|_a$ the velocity, T_a the air temperature, and q_a the air specific humidity, all at the surface. To obtain τ_{qs} and τ_{Ts} from Eqs. (24) and (25), T_a, q_a, and the temperature T_{af} and specific humidity q_{af} for air within the canopy must be known.

It is assumed that the heat capacity of air within the canopy is negligible. Thus, the heat flux from the foliage and ground must be balanced by the heat flux to the atmosphere. The value of T_{af} can be calculated through this relationship and is related to the ground temperature T_{g1} in Eqs. (22) and (23). Also, we assume that the canopy air does not store water vapor. Hence, q_{af} can be calculated in a similar manner and is related to the rooting zone, S_{tw}, surface water content, S_{sw}, and water stored on foliage, W_f, defined in Eqs. (19)–(21). The detailed components associated with the surface energy budget are illustrated in Fig. 1.

The drag coefficient C_D is allowed to vary with atmospheric conditions, as well as the roughness length at the surface. It is taken from Dickinson et al. (1986) in the form

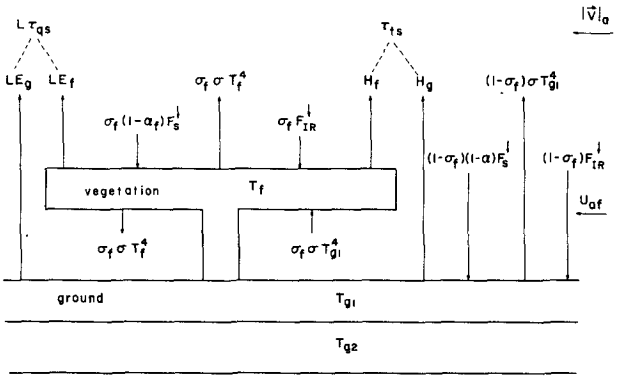

FIG. 1. Schematic diagram denoting the components of the surface energy balance for the vegetation layer and the ground. Here, $F_s^{\downarrow}$ is the solar flux, $F_{IR}^{\downarrow}$ the IR flux, H_g and H_f the heat fluxes from the ground and foliage, respectively, α the surface albedo, α_f the vegetation albedo, σ the Stefan–Boltzmann constant, L the latent heat, σ_f the vegetation cover, T_f, T_{g1}, and T_{g2} the temperatures of the foliage, at the surface soil, and subsurface, respectively, u_{af} the wind velocity within the foliage layer, τ_{qs} the vertical flux of water vapor from the canopy, and τ_{Ts} the heat flux to the atmosphere from the vegetation layer.

TABLE 1. Sea surface temperatures (K) are computed from the GFDL Atmospheric Circulation Tape Library (Oort 1983).

	45°S	40°S	40°N	45°N
June	282.21	285.82	291.84	289.90
July	279.42	284.03	295.35	292.73

$$C_D = \begin{cases} C_{Dn}[1 + 24.5(-C_{Dn}R_{iB})^{1/2}, & R_{iB} < 0 \\ C_{Dn}/(1 + 11.5R_{iB}), & R_{iB} > 0, \end{cases} \tag{26}$$

where R_{iB} is the surface bulk Richardson number, and the drag coefficient under the neutral condition C_{Dn} may be derived from mixing length theory and has the form

$$C_{Dn} = \left[k/\ln\left(\frac{z_s}{z_0}\right)\right]^2, \tag{27}$$

where the von Kármán constant $k = 0.4$, z_0 is the roughness length, and z_s is the height of the surface layer and is specified as 10 m over water and 30 m over land (Hansen et al. 1983).

e. Numerics

The meridional grid extends from 45°S to 45°N and uses a 5°-latitude staggered grid on which the temperature, specific humidity, and horizontal velocity are calculated. The vertical velocity is calculated at midpoints. A vertical pressure coordinate system is used, in which the atmosphere is divided into 19 layers extending to 100 mb. The temperature, specific humidity, and horizontal velocity are calculated at every 50 mb, and the vertical velocity is calculated at midlevels. The time step used is 15 minutes. Solar radiation is calculated once per hour, however, and infrared radiation is calculated once every four hours. We have also used a 2.5°-latitude grid in the numerical calculations and found that the simulation results for model variables do not deviate significantly from those computed from a 5°-latitude grid. To economize the numerical calculations, we have used the latter grid system in climate experiments.

The space differencing for the governing equations employed in the present model is a second-order explicit finite-difference scheme. This numerical method is based on the energy conserving difference scheme described by Haltiner and Williams (1980); however, improvements and refinements have been made in this study. For time differencing in the governing equations, the scheme proposed by Matsuno (1966) is used. For the soil-vegetation layers, a simplified Adams–Bashforth scheme (Lambert 1972) is adopted. A detailed presentation of the two-dimensional climate model, including surface processes, can be found in Xue (1988).

3. Numerical results and discussions

a. Design of the experiment and data source

In our sensitivity study, we use data from the Geophysical Fluid Dynamics Laboratory (GFDL) Atmospheric Circulation Tape Library (Oort 1983) for initial values. These data, including temperature, humidity, and wind fields, are given for every 2.5° latitude and 5° longitude, and are based on a ten-year mean (1963–73). The zonally averaged data for June are used as the initial values. Zonally averaged data were also used to obtain the July values over the African continent for comparisons with the model results computed from control runs. Sea surface temperatures are specified in the model according to the climatological values for the South Atlantic Ocean and the Mediterranean Sea from the GFDL data tape. They are allowed to change from June to July. These values are shown in Table 1.

A thin vegetation layer is assumed between the lowest pressure level and the surface. Different vegetation types are used to characterize a variety of thermal, hydrological, and radiative properties of the surface. The types of vegetation and albedo in each latitude over Africa are based on the data prepared by Matthews (1985). There are 32 vegetation types in Matthews' data, but only 18 were used in parameterizations by Dickinson et al. (1986). To use their values in model simulations, the 32 vegetation types have been combined and reduced to 18 types. From these 18 types, vegetation parameters in each latitude from 45°S to 45°N over Africa may then be calculated. The values for the relevant vegetation parameters are listed in Table 2. In this table, σ_{fs} denotes the maximum fractional vegetation cover and $\Delta\sigma_{fs}$ the seasonal range for each type of vegetation. The albedo values are based on the albedo data for summer seasons presented by Matthews (1985). The zonally averaged albedos for vegetation cover for each grid point over the African continent are listed in Table 3. The albedo for soil is a function of the soil moisture. According to Deardorff (1978), it may be parameterized in the form

$$\alpha = \begin{cases} 0.14, & \text{for } S_{sw} > 0.05 \\ 0.31\text{–}0.17\,(S_{sw}/0.05), & \text{for } S_{sw} < 0.05, \end{cases} \tag{28}$$

where S_{sw} denotes the surface water content. Based on Matthews' data, the area between 17.5°N and 32.5°N is set as desert in the model, and the soil type is taken to be sandy. For other areas, the surface is assumed to be loam-like soil. The surface albedo for each grid point is then the area average of the albedos for vegetation and bare soil. The ocean areas are set north of 37.5°N and south of 37.5°S. As described previously, sea surface temperatures are specified in the 2-D model using climatological data. It should be noted that the surface albedo and other surface properties over the oceans differ significantly from those over land. The solar ze-

TABLE 2. Vegetation parameters.

Latitude	45°S	40°S	35°S	30°S	25°S	20°S	15°S	10°S	5°S	0°
σ_{fs}	0	0	0.810	0.806	0.800	0.803	0.802	0.805	0.832	0.859
$\Delta\sigma_{fs}$	0	0	0.279	0.266	0.229	0.235	0.277	0.289	0.324	0.592
Roughness length z_0	2.3E − 4	2.3E − 4	0.370	0.360	0.670	0.710	0.860	0.890	1.100	1.450
Maximum LAI	0	0	6	6	6	6	5.800	6	6	6
Minimum LAI	0	0	2.700	1.740	2.400	2.520	1.400	1.580	3.020	3.860
Stem area index	0	0	2	2	2	2	2.100	2	2	2

Latitude	5°N	10°N	15°N	20°N	25°N	30°N	35°N	40°N	45°N
σ_{fs}	0.851	0.803	0.805	0	0	0	0.803	0	0
$\Delta\sigma_{fs}$	0.315	0.237	0.233	0	0	0	0.268	0	0
Roughness length	1.110	0.770	0.760	0.01	0.01	0.01	0.850	2.3E − 4	2.3E − 4
Maximum LAI	6	6	6	0	0	0	5.160	0	0
Minimum LAI	3.180	2.450	2.730	0	0	0	3.250	0	0
Stem area index	2	2	2	0	0	0	2.420	0	0

TABLE 3. Surface albedo for vegetation cover and zenith angle.

Latitude	45°S	40°S	35°S	30°S	25°S	20°S	15°S	10°S	5°S	0°
Summer albedo	0.110	0.110	0.230	0.247	0.221	0.190	0.176	0.177	0.153	0.142
Zenith angle	0.4501	0.4821	0.580	0.5339	0.5565	0.5753	0.5904	0.6015	0.6080	0.6364

Latitude	5°N	10°N	15°N	20°N	25°N	30°N	35°N	40°N	45°N
Summer albedo	0.177	0.197	0.255	0.300	0.300	0.300	0.211	0.070	0.070
Zenith angle	0.6090	0.6034	0.5933	0.5791	0.5613	0.5396	0.5145	0.4827	0.4518

nith angles are calculated from the solar inclination, latitude, and hour angle (Liou 1980). The cosines of the solar zenith angles at different latitudes that are used are included in Table 3.

In Table 4 we list the numerical experiments performed in the study. In addition to the control runs, we carry out simulations that involve removing and expanding the desert. We also add experiments that allow only the albedo to vary. The objective of these computations is described below.

b. Results of control runs

The primary objective of the control runs is to validate the model and associated physical parameterizations. In most African drought simulation studies, July was chosen to test the sensitivity of the surface feedback to precipitation. This is due to the fact that during the northern summer there is more rainfall and larger solar flux in the Sahel. Thus, a maximum response could be expected in this month. In the experiment described herein, the June global average climate data were used as initial values. The time integrations of the model were carried out for 45 days. The results for the last 30 days were averaged in order to compare them with the GFDL data over Africa for July conditions.

The computed temperature field for the African continent is shown in Fig. 2b. In general, the model-simulated temperatures reproduce the observations displayed in Fig. 2a. Between 800 and 400 mb, the temperature differences in most areas are less than 1 K. In the upper troposphere, larger differences between the computed and observed temperatures on the order of 2–5 K are seen in the Northern Hemisphere. The maximum temperature near the ground is located between 20° and 30°N, as illustrated in Fig. 2b. The simulated maximum shifts slightly to the north. This coincides with the assumed desert area. The temperatures near the surface in the simulation are generally colder by 2–4 K. One of the reasons for colder temperatures near the surface might be enhanced infrared flux exchanges since the model atmosphere is generally wetter (see the discussion below).

Four systems in the African July zonal wind cross section are observed in the climatological data presented in Fig. 3a. In the upper troposphere there are middle latitude westerlies in both hemispheres and

TABLE 4. Classification of the numerical experiments.

Case	Classification
a	Control run
b	Desert expanded to 10°N
c	Desert removed
d	Desert expanded but with albedo change only
e	Desert removed but with albedo change only

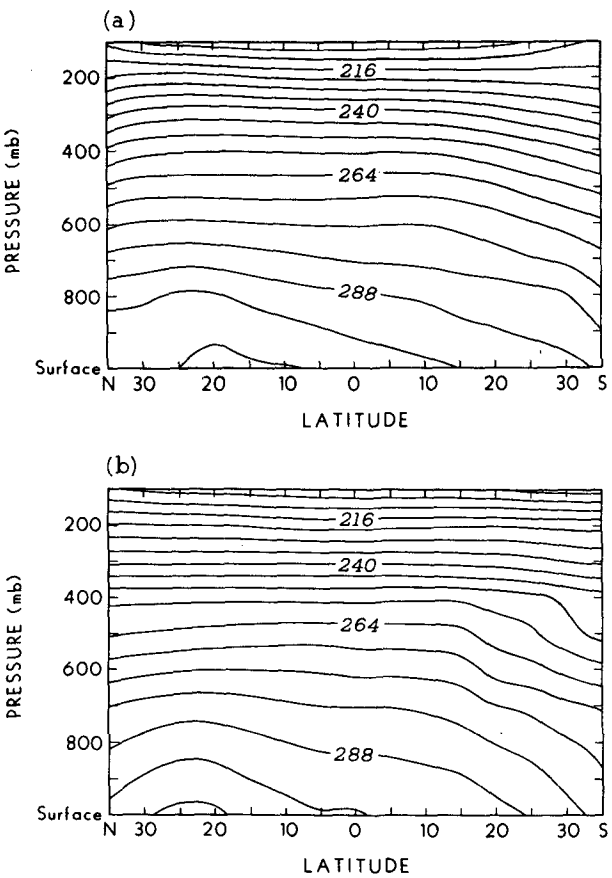

FIG. 2. July zonal average temperature (K) over Africa: (a) observed (Oort 1983) and (b) control run. The contour interval is 6 K.

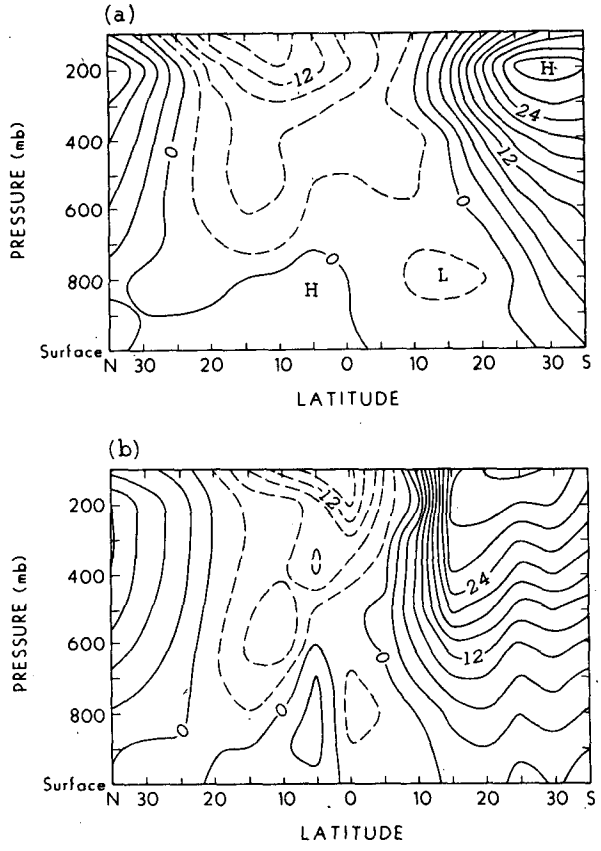

FIG. 3. July zonal average zonal velocity (m s^{-1}) over Africa: (a) observed (Oort 1983) and (b) control run. The contour interval is 3 m s^{-1}.

tropical easterlies. Between 2.5°S and 22.5°N, there are westerlies at low levels. These four systems are reproduced in the model simulations, as is evident in Fig. 3b. The zonal westerlies simulated by the model have two maxima. The maximum location at 100 mb is slightly high when compared to observed values. Also, the simulated northern maximum is about 200 mb too low. This displacement may be related to the production of the thermal wind due to the shift of the maximum temperature gradient towards the equator in the control run, as shown in Fig. 2.

The atmosphere is wetter in our simulations, probably due to excessive evaporation from the ground produced by the model. The computed specific humidity maximum at the ground is 5° north of the climatological data (Figs. 4a and 4b). This is consistent with the differences between the computed and observed surface temperature maximum. From the observations, there is more water vapor in the Northern Hemisphere than in the Southern Hemisphere. This is reproduced by the model. There is a dry trough above the desert in the observations (Fig. 4a). In the simulations, the dry trough is quite pronounced below 700 mb. The simulated specific humidity also shows a trough near the surface at 10°S, consistent with the sinking motion in the model. This phenomenon, however, is not significant in the observations. The African continent is narrow in the Southern Hemisphere. Due to zonal advections, ample moisture could be supplied to the land by the oceans. This mechanism is not accounted for in the 2-D model. Near the southern boundary, there are large horizontal gradients in the computed water vapor mixing ratio profile because of the imposed boundary condition of no horizontal flux.

The simulated precipitation is shown in Fig. 5, along with the climatological data from Schutz and Gates (1972). The precipitation simulated by the model generally agrees well with that from climatology. The precipitation pattern shows a maximum near the equator and two minima, located in the Sahara Desert and a region between 10° and 20°S. Considering the uncertainty in observed precipitation data, the present results are quite encouraging.

The preceding discussion illustrates that the present 2-D model can, in general, simulate the observed zonal mean features over Africa. Because the simulations are based on a 2-D model, it is not expected that the model

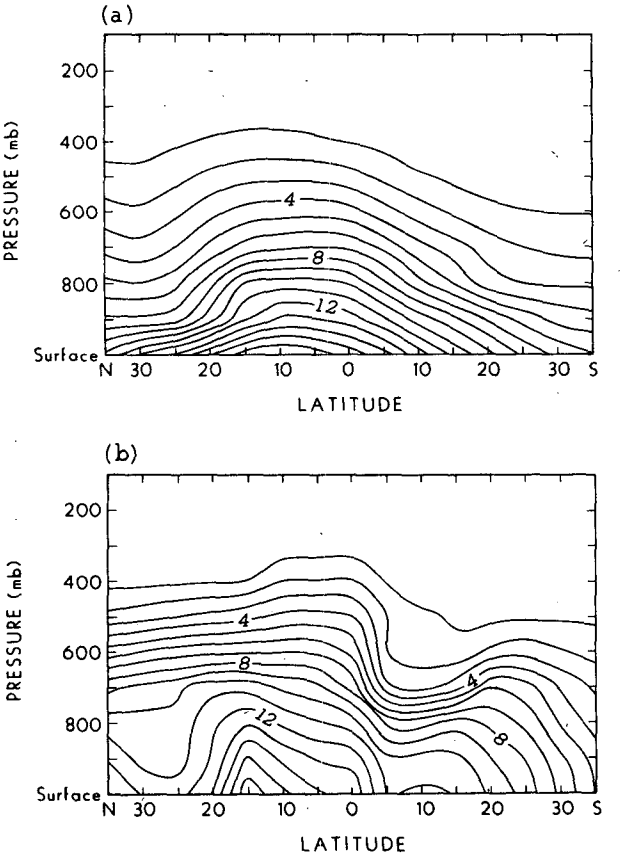

FIG. 4. July zonal average specific humidity (g kg^{-1}) over Africa: (a) observed (Oort 1983) and (b) control run. The contour interval is 1 g kg^{-1}.

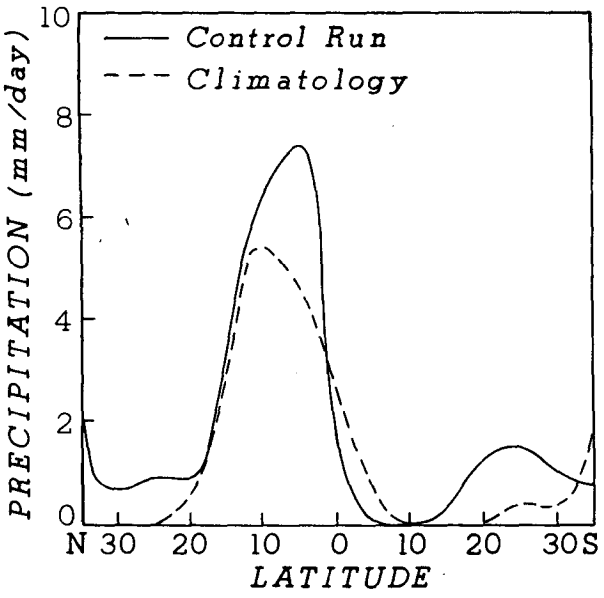

FIG. 5. July rainfall distribution (mm day^{-1}) over Africa for the control run and climatology.

would reproduce the observed features exactly. The computed results in the Northern Hemisphere seem to be better than in the Southern Hemisphere. This may be due to the fact that the geography of northern Africa is more zonal and the influence of orography is less in the Northern Hemisphere.

c. *Sensitivity experiments*

The most significant climatic feature in Africa is undoubtedly rainfall. According to the historical climate record, there have been several drought periods, followed by wet periods (Nicholson 1985). During the period from 1820 to 1920, there were three rainfall anomalies, including two dry periods and one wet period. Each of these periods persisted for about 25 years. Lamb (1985) studied the rainfall patterns in western Africa for the period from 1941 to 1983. His climatological analyses show that the years 1950–60 were wetter than normal, whereas the years 1970–83 were drier than normal.

Extensive efforts have been made in the past to investigate the relationship among the African drought, temperature, and the mean general circulation, based on data analysis. For example, in the years with low rainfall, the temperature is higher at the surface (Tanaka et al. 1975). Higher temperatures were also reported by Kidson (1977) at the 850 and 500 mb levels. Nicholson (1981) found that a northward displacement of the ITCZ may account for the wetter years in the Sahel, but the ITCZ is a less significant factor in the Sahel droughts. These results differ from those experiments in which only the albedo is changed in the model studies.

Kanamitsu and Krishnamurti (1978) and Newell and Kidson (1984) indicated that during dry years the zonal easterly winds at 200 mb in the near-equatorial tropical belt are weaker, but the westerlies in the middle latitudes are stronger than normal. In addition, there are a number of other investigations that attempt to relate changes in Sahel rainfall to changes in the general circulation; however, the results are not particularly convincing. Using the present model, two experiments were performed to investigate the response of surface conditions to the African drought. The desertification in Africa occurred primarily in the Sahel area. To test the feedback of surface parameters to the climate, the desert is extended to 10°N. This extension is designed to exaggerate the actual desertification in order to ensure computational significance. The surface albedo of the extended desert is changed according to Eq. (28) ($\sim$0.3) with no vegetation cover. The soil type is modified to sandy conditions. Note that the exact surface albedo value varies with soil moisture. The roughness length is set to 0.01 m. The albedos for vegetation at 10° and 15°N are 0.197 and 0.255, respectively, as listed in Table 3. To obtain the average surface albedo before desertification, it is necessary to weight the albedos for vegetation cover and bare soil according to the area coverage. The surface albedo increases by about 0.07 (or $\sim$34%) in the desertification experiments. It should be noted that the increase in the surface albedo is reasonable, but the extension of the desert to 10°N is an exaggeration, as pointed out previously. This exaggeration allows us to investigate the interactions and feedbacks between the surface processes and the atmosphere, and should not be viewed as what actually occurred in Africa.

Another experiment is performed in which the desert in the Sahara area is removed. The vegetation albedo, roughness, and vegetation cover used are set to 0.17, 0.75, and 0.8, respectively. The initial soil moisture is set to 2 cm on the surface and 25 cm in the total soil layer in vegetation areas. In the desert area, 1 and 10 cm are used for these soil moisture values.

1) DESERT EXPANDED

After the desert expanded, precipitation, cloud cover, and evaporation changed significantly. The distributions of precipitation, evaporation, and cloud cover are shown in Figs. 6a–c, respectively. The total precipitation for the entire area decreases by about 13%. The decrease occurs primarily in the desertification area and Sahara region. The evaporation and cloud cover are also reduced in these areas. The reductions in rainfall, evaporation, and cloud cover in the expanded desert area (10° $\sim$ 20°N) are 1.5 mm day^{-1}, 1.7 mm day^{-1}, and 0.07, respectively. The net radiation at the top of the atmosphere in the expanded desert area decreases by about 10 W m^{-2}. The deficit for the solar flux is about 11 W m^{-2} in that area. This implies that

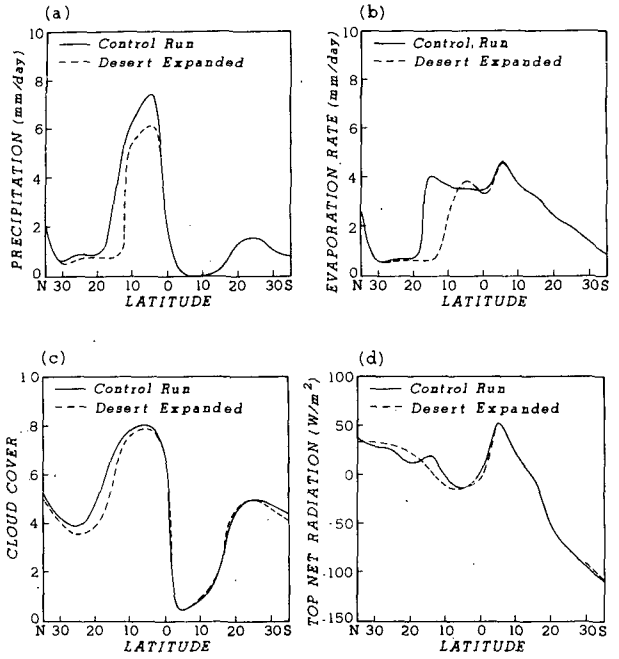

FIG. 6. Comparison between results computed from the control run and desert expanded run with the July mean: (a) rainfall, (b) evaporation, (c) cloud cover, and (d) net radiation at the top of the atmosphere.

the thermal infrared flux does not change significantly. In the entire area, the loss of solar fluxes is almost compensated for by the increase in thermal infrared fluxes due to surface temperature increases (Fig. 6d).

The time series for the perturbed precipitation, evaporation, and runoff in the expanded desert area are shown in Fig. 7b. For comparison, the results from the control run are displayed in Fig. 7a. The differences between the perturbed and control runs are due not only to the reduction in soil moisture and the absorbed solar flux, but also to the change in soil type and the elimination of vegetation cover. When the soil type changes from loam-like to sandy, the saturated soil suction decreases by about one-seventh. As a result, the down-gradient rate TR [see Eq. (19)] of transfer of water from the lower soil layer to the surface layer is reduced because it is proportional to the soil suction. Subsequently, the evaporation rate from the soil surface is also decreased. At the same time, the water is unable to transpirate from the soil without vegetation. Thus the total evaporation rate from the surface decreases, as shown in Fig. 7. The subsoil drainage R_g [see Eq. (20)] is proportional to the saturated soil hydraulic conductivity, which is much larger for sandy soil than for loam-like soil. For this reason, more water would be able to leak down to the subsoil layer in the case of sandy soil. Although the surface runoff decreases, we find that the total runoff increases slightly when the desert is expanded, as illustrated in Fig. 7.

Besides the change in latent heat release, convergence of the horizontal water vapor transport could also lead to the redistribution of rainfall. In Fig. 8, we examine the change in the convergence of the horizontal water vapor transport computed from perturbed and control runs. In the expanded desert area, a slight increase in water vapor convergence is seen near the surface layer due to the warmer surface; however, a significant divergence is produced above the surface and below about 700 mb, with a maximum value of about 0.2 mm day^{-1} located at 800 mb. Using a GCM, Sud et al. (1988)

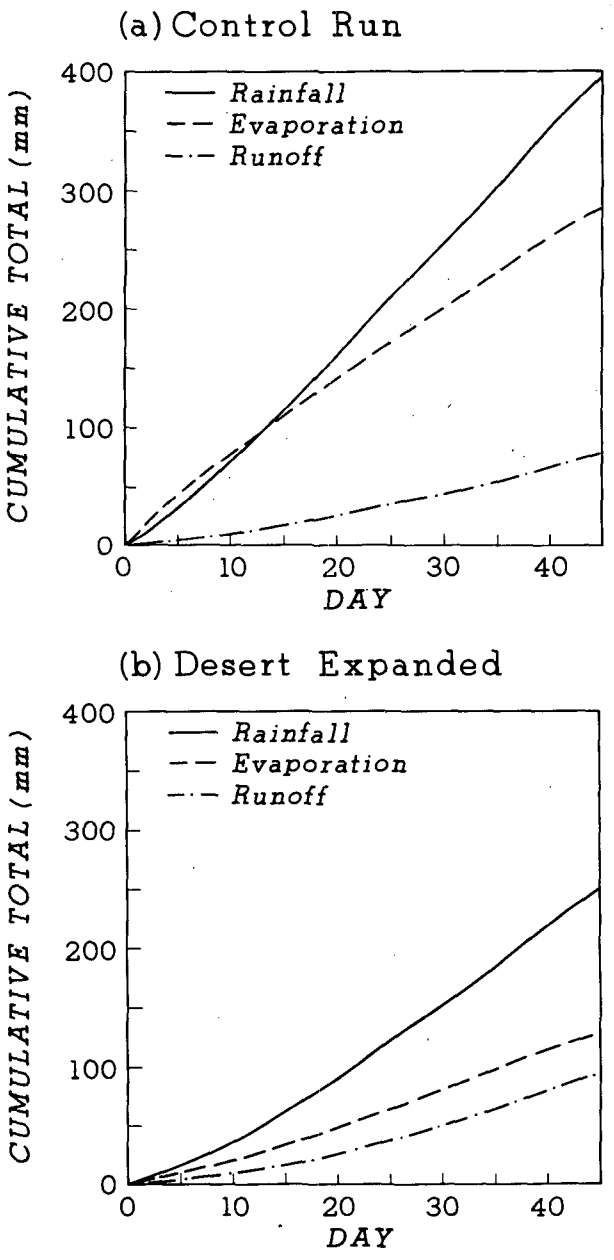

FIG. 7. Precipitation, evaporation, and runoff as functions of day for 45 days for control and desert expanded runs.

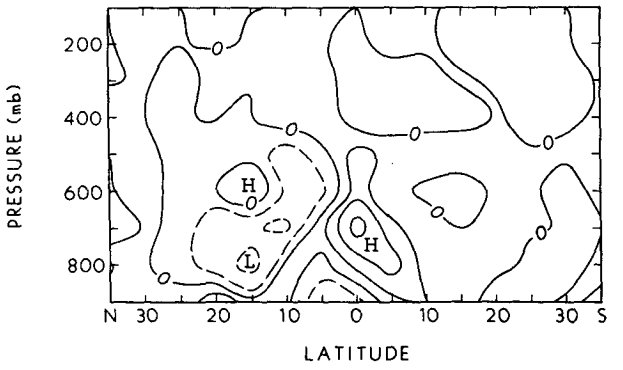

FIG. 8. Differences in the horizontal convergence of water vapor (mm day^{-1}). The contour interval is 0.05 mm day^{-1}.

also found that water vapor convergence is closely associated with the land surface parameters. It should be noted that because of the limitation of the 2-D model, the potential horizontal transport of water vapor in the east–west direction cannot be accounted for. It is conceivable that if the oceans were at the same latitude as the desertification areas, the horizontal convergence of water vapor could differ from the present results. The role of the oceans in the desertification of Africa is a subject requiring further investigations using an appropriate GCM.

In the expanded desert area, the atmospheric temperatures increase in low levels, as well as at levels above 400 mb. Shown in Fig. 9a are the temperature differences between expanded desert and control cases. The present results agree with the conclusion reported by Kidson (1977). Based on observations, he indicated that higher temperatures at 850 mb and at the surface are associated with lower rainfall in the Sahel. The surface temperature increase (~1 K) in the expanded desert area from model calculations is lower than the observed values over the Sahel in dry years, as reported by Tanaka et al. (1975), by less than 1 K. There is slight cooling in the upper atmosphere caused by a reduction in net radiation (see Fig. 6d), as proposed by Charney (1975).

In Fig. 9b, zonal wind differences are shown. The westerly zonal winds become slightly stronger in the expanded desert run in southern midlatitudes, whereas the easterly zonal winds weaken at 200 mb. Based on the data for a wet year (1967) and a dry year (1972), Kanamitsu and Krishnamurti (1978) reported that the westerlies in both hemispheres are stronger in a dry year. Based on the data analyzed for the periods 1958–62 (wet years) and 1970–73 (dry years), however, Newell and Kidson (1984) illustrated that the westerlies are strong only in the Southern Hemisphere. Our simulation results agree with the latter finding.

The physical processes through which the surface influences the atmosphere are schematically displayed in Fig. 10. The values in this figure correspond to expanded desert areas only. When the desert expands, the albedo of the total expanded area increases by about 0.07 (~34%). This leads to a decrease in net solar fluxes at the ground. Because the amount of cloud cover is smaller, the net solar flux only decreases by 8%. As a result of less net radiative flux, the sum of latent and sensible heat also decreases. The sensible heat becomes larger since the ground temperature increases due to desertification. The reduction in the water source results in less evaporation. It follows that the latent heat changes dramatically. This will ensure that the sum of latent and sensible heat has the same sign as the net radiative fluxes. In addition, the drag coefficient decreases. The roughness length z_0 decreases from 0.8 to 0.01 m after desertification, as specified in the present study. This leads to a decrease in the drag coefficient C_D by about one order of magnitude. This effect is partly compensated for by the larger surface wind speed v_a, which could be related to the wind storms commonly observed in desert areas. The change in surface parameters further leads to a reduction in the horizontal convergence of water vapor. The reduction in evapo-

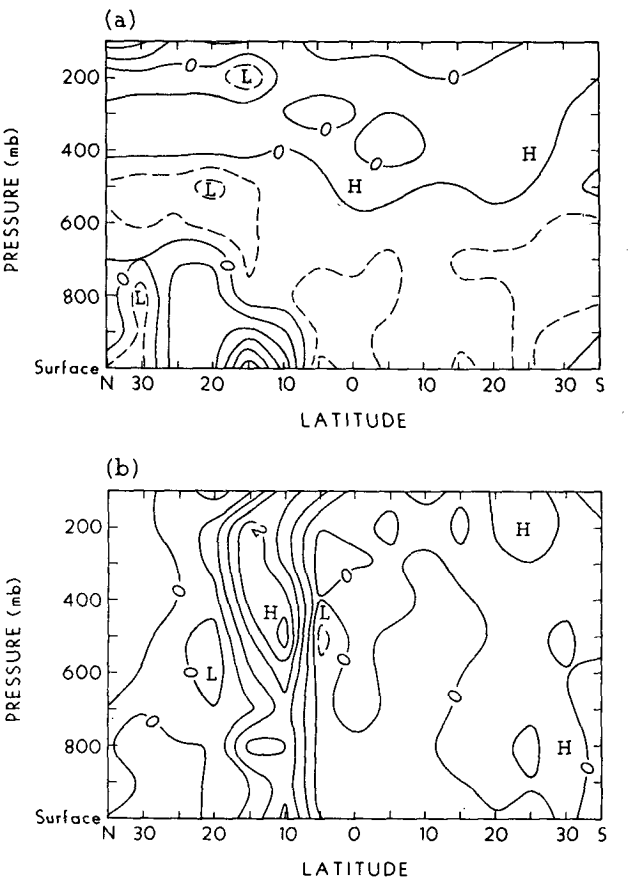

FIG. 9. Differences between Cases b and a (see Table 4 for identification): (a) temperature (K) and (b) zonal velocity (m s^{-1}). The contour intervals for temperature and zonal velocity are 0.25 K and 0.5 m s^{-1}, respectively.

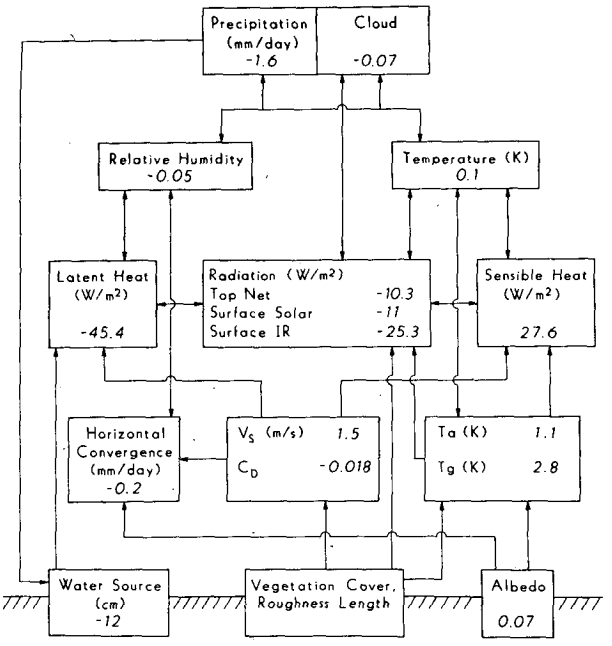

FIG. 10. Differences in various physical quantities between the desert expanded b and control runs a, illustrating the interactions and feedbacks of the surface processes to the climate system (see Table 4 for the case identification).

ration and the horizontal convergence of water vapor coupled with the increase in atmospheric temperatures result in less relative humidity, and hence, less precipitation and cloud cover.

2) DESERT REMOVED

In this experiment, the Sahara Desert is removed. The removal of the Sahara Desert increases precipitation by about 25% averaged over the entire model area. In the Sahara area, however, the increase is much more pronounced (~320%), as shown in Fig. 11a. The rainfall decreases south of this area, which agrees with the results presented by Charney et al. (1977). In their study, the increase in rainfall in the Sahara in the low albedo experiment is compensated for by a decrease south of the Sahara. In fact, Nicholson (1981) also found from the climatological data analysis that rainfall anomalies are frequently of opposite sign north and south of 10°N. The cloud cover shown in Fig. 11b increases by 52% in the Sahara area. More evaporation is evident in the Sahara where evaporation is 3.2 mm day^{-1} more than that produced in the control run. Differences in evaporation are shown in Fig. 11c. The net radiation at the top of the atmosphere also increases, as shown in Fig. 11d. It increases by about 2.0 W m^{-2} in the entire model domain. In the Sahara, the increase is about 10 W m^{-2}.

The removal of the Sahara Desert generates a cooler atmosphere in that area below about 750 mb. The maximum cooling occurs in the desert removed area, but the temperatures are higher in the upper atmosphere. The westerlies in the southern midlatitudes decrease, and the tropical easterlies become stronger near 200 mb.

Figure 12 shows a schematic relation for the feedback between various processes when the desert is removed and replaced by a vegetation layer. The feedback processes are similar to those presented in Fig. 10, except that the + and − signs are reversed. The values are larger because we have changed three grid points in this case (i.e., the entire Sahara is removed) instead of two in the desert expanded areas.

d. The effects of soil moisture and vegetation

To understand more comprehensively the influence of vegetation cover and soil moisture, an additional two experiments were performed, as listed in Table 4. In these tests, the albedo is the only parameter that varies. The differences in precipitation, cloud cover, and evaporation produced from various cases are listed in Table 5. For comparison purposes, the results computed from changing the vegetation cover are also presented in this table.

Two entries are presented for each item: one, called Test, lists the results corresponding to the surface area that was changed in the experiment, while the other, called Entire, is associated with the whole domain used in the experiment. From this table, we find that the response in the whole domain has the same sign as that in the local area, but it is smaller. In Case d, when the albedo increases, precipitation decreases. The decrease in precipitation is less than in the case when the vegetation layer is coupled in the model.

As shown in Table 5, the major differences are in the sign of the sensible heat change. The sensible heat change is negative as the desert is expanded, because the ground temperature decreases if only the albedo is allowed to vary. When vegetation variation is included in the experiment, however, the sensible heat change is positive. In Case e, the change in sensible heat is even larger than that in latent heat. Sensible heat plays a more important role than latent heat in the case when only the albedo is varied. This differs from the results when the vegetation cover is removed or added in the experiment.

The changes in temperature when the desert is expanded are shown in Fig. 13a. In this case, the reduction in the transfer of sensible and latent heat to the atmosphere leads to cooling, which in turn either increases low-level horizontal divergence and sinking motions or reduces low-level horizontal convergence and rising motions. When vegetation cover changes, a reduced solar flux does not lead to surface cooling because evaporation also decreases. In Case b the ground temperature in the desertification area is about 2 K higher than that in the control run.

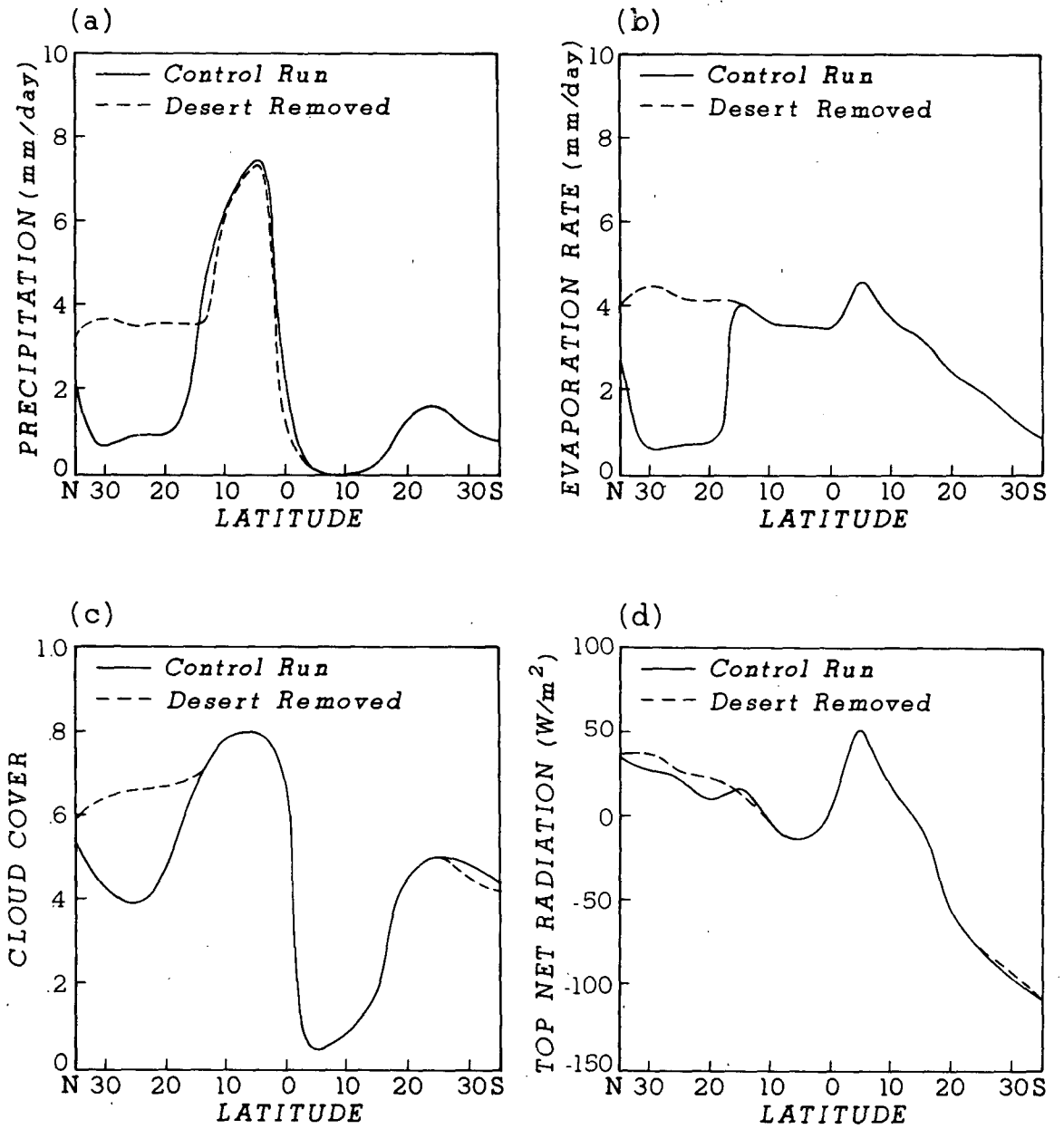

FIG. 11. Comparison between the results computed from the control run a and desert removed run c: (a) precipitation, (b) evaporation rate, (c) cloud cover, and (d) net radiation at the top of the atmosphere.

Figure 13b shows the differences in the horizontal convergence of water vapor. The contour in this figure is 0.06 mm day^{-1}. The largest reduction of about 0.2 mm day^{-1} is produced in the desertification area. This reduction is quite significant in comparison with the total precipitation decrease of 0.5 mm day^{-1}. In this case, the perturbed zonal winds in the experiments are no longer consistent with observations.

In the experiments that coupled vegetation layers, the response is more complex. The sinking motions in these experiments are produced near the desertification area, not exactly over it. The dry and heated ground usually produces a rising motion there. It is clear that numerous factors besides sinking motions would influence precipitation patterns. For example, the moisture content of the air is very important for the production of precipitation. If there is insufficient moisture in the environment, a rising motion is unlikely to produce precipitation. Figures 14a and 14b show the difference in the specific humidity when the desert is expanded, corresponding to Cases b and d, respectively. From Fig. 14, it can be seen that the specific humidity

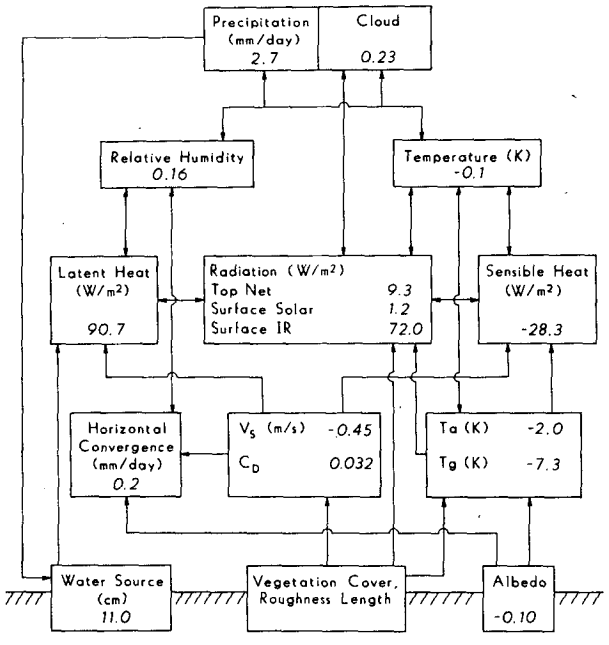

FIG. 12. Same as Fig. 11, except for the desert removed run c.

decreases near the desertification area much more significantly when vegetation and moisture are allowed to vary in the experiment.

Another important factor that influences rainfall is the circulation, which directly affects the advection of water vapor. From the results of the present study, it is found that occasionally the largest reduction in precipitation occurs not only in the anomalous area, but also in some other regions. The cloud patterns produced from the desert expanded experiment remain about the same as those from the control run. Based on observations, Nicholson (1981) indicated that the ITCZ does not vary significantly in dry years. The results presented in this study are in general agreement with Nicholson's findings.

TABLE 5. Differences in fluxes (W m^{-2}), precipitation, evaporation, and cloud cover between experimental and control runs.

Case		b	d	c	e
Net radiation at the top	Test	−10.3	−22.9	9.3	21.1
of the atmosphere	Entire	−0.17	−2.3	1.5	3.8
Net shortwave flux at	Test	−11.0	−28.5	1.2	27.1
the ground	Entire	0.5	−2.9	0.4	5.2
Net longwave flux at	Test	−25.3	−11.2	72.0	−8.7
the ground	Entire	−3.8	−0.5	12.9	−2.0
Sensible heat	Test	27.6	−3.7	−28.3	16.4
	Entire	5.3	−0.1	−4.8	2.8
Latent heat	Test	−45.4	−31.6	90.7	2.3
	Entire	−7.9	−2.8	16.0	−0.2
Precipitation	Test	−1.58	−1.0	2.73	0.08
(mm day^{-1})	Entire	−0.27	−0.1	0.52	0
Cloud cover (%)	Test	−0.07	−0.02	0.23	0.01
	Entire	−0.02	0	0.04	0

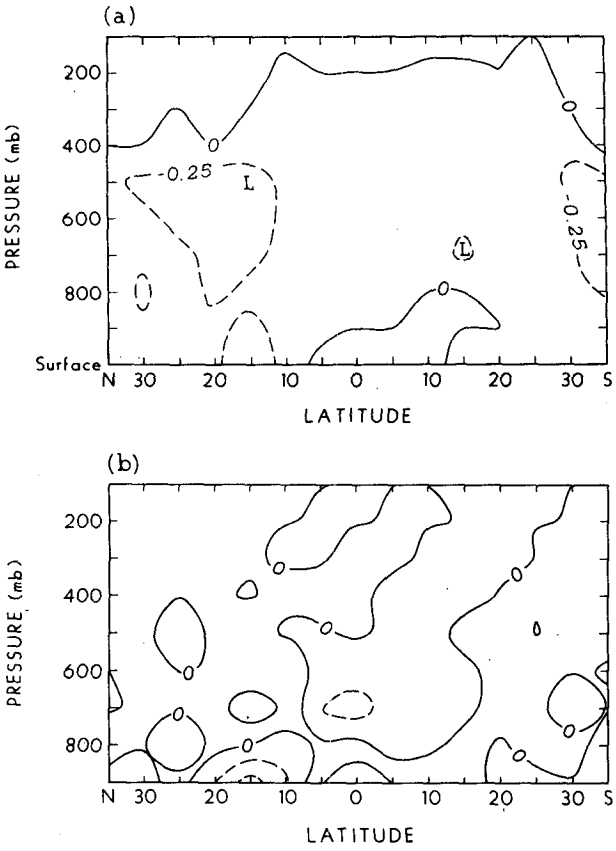

FIG. 13. Differences between Cases d and a (see Table 4 for the case identification): (a) temperature (K) and (b) the horizontal convergence of water vapor (mm day^{-1}). The contour intervals for these two variables are 0.25 K and 0.06 mm day^{-1}, respectively.

4. Conclusions

In this paper, a 2-D model has been developed to study the interaction between surface characteristics and the atmospheric circulation over the African region. A soil–vegetation layer has been introduced in the model for this purpose. In the control runs, the general features of the July African zonal patterns are simulated. In the perturbation runs, surface processes significantly affect the precipitation, cloud cover, temperature, and wind velocity patterns. As the desert is expanded, precipitation and cloud cover are reduced. At the same time, the temperature increases, and the westerly winds become stronger. When the desert is removed and replaced by a vegetation layer, however, the opposite occurs. The results appear to be in general agreement with the observed features of Africa's dry and wet years.

To investigate the feedback mechanisms of various physical processes in the model, numerical experiments have been carried out. In one of the experiments, only the albedo is varied in the simulation. This experiment produced almost the same results as those presented

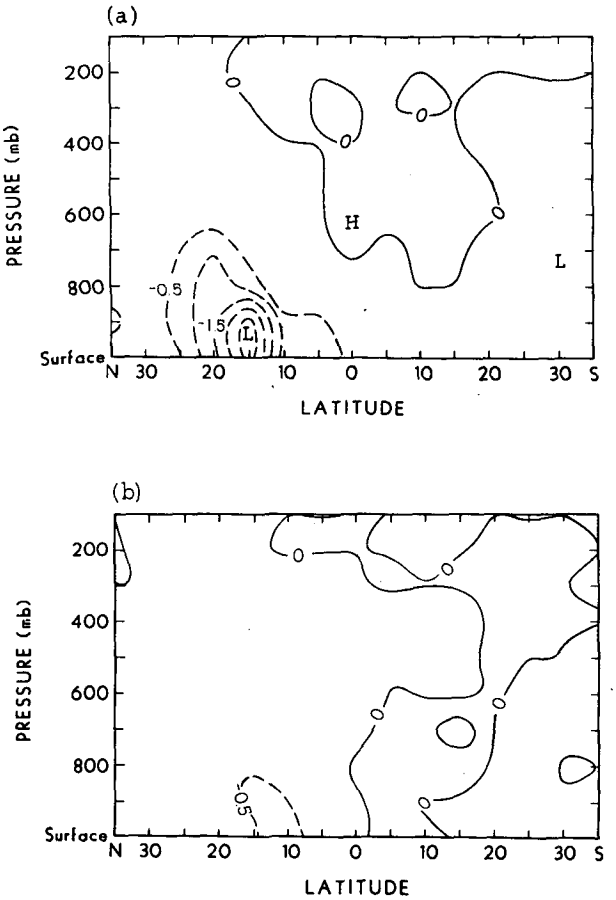

FIG. 14. Specific humidity differences (g kg^{-1}) for: (a) Cases b–a and (b) Cases d–a (see Table 4 for the case identification).

by Charney (1975) and Charney et al. (1975). When the albedo is increased, the temperature is reduced, leading to a stronger horizontal divergence of the water vapor transport. As a result, rainfall decreases. The response with the albedo change only is less than the response when the vegetation layer is included in the model. Without the incorporation of interactive changes in the vegetation layer, the circulation patterns produced do not agree with observations. An examination of surface energy budgets reveals that if only the albedo is altered, the simulated change in sensible heat is occasionally larger than in latent heat. In this case, both the changes in sensible and latent heat components have the same sign. This differs from simulation results when the vegetation cover change is incorporated in the model. In the latter case, the change in latent heat is the dominant factor, significantly affecting precipitation, cloud cover, energy budgets, and circulation patterns.

Vegetation affects latent and sensible heat through not only surface temperature and humidity, but also surface wind and drag coefficients. When vegetation is introduced, surface winds are smaller than in the case for bare soil. The drag coefficients are much larger, however, by about an order of magnitude. This would produce a larger vertical flux of heat and moisture.

It is not the intent of this study to simulate the African climate exactly using a 2-D model and to resolve the complex issue of desertification and drought in Africa. Our objective, however, is to investigate the sensitivity in the physical processes of the atmosphere–soil boundary layer to changes in surface conditions to further our understanding of the mechanisms and feedbacks associated with African drought.

The present sensitivity study of desertification and drought in Africa is subject to two assumptions, namely, that the desert is expanded to 10°N, and that only meridional advection is important due to the limitation of the 2-D model. While we are able to demonstrate the importance of vegetation cover and soil moisture on the temperature, circulation, and precipitation over Africa, the role of the oceans has not been addressed in this paper. The latter issue requires further investigation using an appropriate and detailed GCM. Subject to the aforementioned assumptions, we find that the atmospheric conditions simulated in this study appear to be in general agreement with climatological data for dry years presented by a number of researchers. It seems reasonable to suggest that desertification in the Sahel area could be one of the major factors linked to African drought.

Finally, based on the present study, we find that changes in the vegetation layer influence not only the albedo, but also the surface hydrology. At the same time, through various processes, these changes also affect the surface energy balance. Thus, it is important to incorporate the physics of a vegetation layer in the investigation of biogeophysical feedbacks.

Acknowledgments. This research was supported, in part, by NASA Grants NAG-732 and NAG-1050, the Air Force Office of Scientific Research Grant AFOSR-87-0294, and NOAA Grant NA85 AAG02575. All the computations were carried out at the National Center for Atmospheric Research, which is sponsored by the National Science Foundation. We thank Dr. R. Dickinson for his helpful comments and suggestions on the paper.

REFERENCES

Charney, J. G., 1975: Dynamics of deserts and drought in the Sahel. *Quart. J. Roy. Meteor. Soc.*, **101**, 192–202.

——, P. H. Stone and W. J. Quirk, 1975: Drought in the Sahara: A biogeophysical feedback mechanism. *Science*, **187**, 434–435.

——, W. J. Quirk, S.-H. Chow and J. Kornfield, 1977: A comparative study of the effects of albedo change on drought in semi-arid regions. *J. Atmos. Sci.*, **34**, 1366–1385.

Deardorff, J. W., 1972: Theoretical expression for the countergradient vertical heat flux. *J. Geophys. Res.*, **77**, 5900–5904.

——, 1978: Efficient prediction of ground surface temperature and moisture with inclusion of a layer of vegetation. *J. Geophys. Res.*, **83**, 1889–1908.

Dickinson, R. E., 1984: Modeling evapotranspiration for three-dimensional global climate models. *Climate Processes and Climate Sensitivity,* Geophysical Monograph, 29, J. E. Hansen and T. Takahashi, Eds., American Geophysical Union, 58–72.

——, and A. Henderson-Sellers, 1988: Modelling tropical deforestation: A study of GCM land-surface parameterizations. *Quart. J. Roy. Meteor. Soc.,* **114,** 439–462.

——, J. Jager, W. M. Washington and R. Wolski, 1981: Boundary subroutine for the NCAR Global Climate Model. NCAR/TN-173+1A, 75 pp.

——, A. Henderson-Sellers, P. J. Kennedy and M. F. Wilson, 1986: Biosphere–atmosphere transfer schemes (BATS) for the NCAR community climate model. NCAR/TN-275+STR, 69 pp.

Elsaesser, H. W., M. C. MacCracken, G. L. Potter and F. M. Luther, 1976: An additional model test of positive feedback from high desert albedo. *Quart. J. Roy. Meteor. Soc.,* **102,** 655–666.

Flohn, H., 1972: General climatology. *Climates of Africa,* J. F. Griffiths, Ed., Elsevier, 604 pp.

Geleyn, J. F., 1981: Some diagnostics of the cloud/radiation interaction in ECMWF forecasting model. *Workshop on Radiation, Cloud-Radiation Interactions in Numerical Modeling,* European Centre for Medium-Range Weather Forecasts, Shinfield Park, Reading, U.K., 135–162.

Haltiner, G. J., and R. T. Williams, 1980: *Numerical Prediction and Dynamic Meteorology.* Wiley & Sons, 471 pp.

Hansen, J., G. Russell, D. Rind, P. Stone, A. Lacis, S. Lebedeff, R. Reudy and L. Travis, 1983: Efficient three-dimensional global models for climate studies: Models I and II. *Mon. Wea. Rev.,* **111,** 609–662.

Holloway, J. L., Jr., and S. Manabe, 1971: Simulation of climate by a global general circulation model. *Mon. Wea. Rev.,* **99,** 335–370.

Kanamitsu, M., and T. N. Krishnamurti, 1978: Northern summer tropical circulations during drought and normal rainfall months. *Mon. Wea. Rev.,* **106,** 331–347.

Kidson, J., 1977: African rainfall and its relation to the upper air circulation. *Quart. J. Roy. Meteor. Soc.,* **103,** 441–456.

Lamb, P. J., 1985: Rainfall in sub-Saharan west Africa during 1941–83. *Proceedings of Third Conference on Climate Variations and Symposium on Contemporary Climate 1850–2100,* Los Angeles, 64–67.

Lambert, J. D., 1972: *Computational Methods in Ordinary Differential Equations.* John Wiley & Sons, 278 pp.

Laval, K., and L. Picon, 1986: Effect of a change of the surface albedo of the Sahel on climate. *J. Atmos. Sci.,* **43,** 2418–2429.

Liou, K. N., 1980: *An Introduction to Atmospheric Radiation.* Academic Press, 392 pp.

——, and S. C. S. Ou, 1981: Parameterization of infrared radiative transfer in cloudy atmospheres. *J. Atmos. Sci.,* **38,** 2707–2716.

——, and ——, 1983: Theory of equilibrium temperatures in radiative-turbulent atmospheres. *J. Atmos. Sci.,* **40,** 214–219.

——, —— and P. J. Lu, 1985: Interactive cloud formation and climatic temperature perturbations. *J. Atmos. Sci.,* **42,** 1969–1981.

Matsuno, T., 1966: Numerical integrations of the primitive equations by a simulated backward difference method. *J. Meteor. Soc. Japan,* **44,** 76–84.

Matthews, E., 1985: Atlas of archived vegetation, land-use and seasonal albedo data sets. NASA Tech. Memo. 86199, Goddard Institute for Space Studies, New York, 53 pp.

Newell, R. E., and J. W. Kidson, 1984: African mean wind changes between Sahalian wet and dry periods. *J. Climate,* **4,** 27–33.

Nicholson, S. E., 1981: Rainfall and atmospheric circulation during drought periods and wetter years in west Africa. *Mon. Wea. Rev.,* **109,** 2191–2208.

——, 1985: African rainfall fluctuations 1850 to present: Spatial coherence, periodic behavior and long-term trends. *Proceedings of Third Conference on Climate Variations and Symposium on Contemporary Climate 1850–2100,* Los Angeles, 62–63.

Oliger, J. E., R. E. Wellck, A. Kasahara and W. M. Washington, 1970: Description of NCAR global circulation model. NCAR/TN-56+STR, 93 pp.

Oort, A. H., 1983: Global atmospheric circulation statistics, 1958–1973. NOAA Professional Paper No. 14, U.S. Govt. Printing Office, Washington, D.C., 180 pp. and 47 microfiches.

Potter, G. L., H. W. Elsaesser, M. C. MacCracken and S. Ellis, 1975: Possible climatic impact of tropical deforestation. *Nature,* **258,** 697–698.

Rind, D., 1982: The influence of ground moisture conditions in North America on summer climate as modeled in the GISS GCM. *Mon. Wea. Rev.,* **110,** 1487–1497.

——, 1984: The influence of vegetation on the hydrologic cycle in a global climate model. *Climate Processes and Climate Sensitivity,* Monograph 29, J. E. Hansen and T. Takahashi, Eds., American Geophysical Union, 73–91.

Ripley, E. A., 1976: Drought in the Sahara: Insufficient biogeophysical feedback? *Science,* **191,** 100–101.

Schutz, C., and W. L. Gates, 1972: Global climatic data for surface, 800 mb, 400 mb: July. Rep. R-1029-ARPA, Rand Corporation, Santa Monica, CA.

Sellers, P. J., Y. Mintz, Y. C. Sud and A. Dalcher, 1986: A simple biosphere model (SIB) for use within general circulation models. *J. Atmos. Sci.,* **43,** 505–531.

Shukla, J., and Y. Mintz, 1982; A study of the influence of land-surface evapotranspiration on the earth's climate. *Science,* **215,** 1498–1501.

Sud, Y. C., and M. Fennessy, 1982: A study of the influence of surface albedo on July circulation in semi-arid regions using the GLAS GCM. *J. Climate,* **2,** 105–125.

——, J. Shukla and Y. Mintz, 1988: Influence of land surface roughness on atmospheric circulation and rainfall: A sensitivity study with a general circulation model. *J. Appl. Meteor.,* **27,** 1036–1054.

Tanaka, M., B. C. Weare, A. R. Navato and R. E. Newell, 1975: Recent African rainfall patterns. *Nature,* **255,** 201.

Walker, J., and P. R. Rowntree, 1977: The effect of soil moisture on circulation and rainfall in a tropical model. *Quart. J. Roy. Meteor. Soc.,* **103,** 29–46.

Xue, Y., 1988: Investigation of the biogeophysical feedback on the African climate using a two-dimensional model. Ph.D. dissertation, University of Utah, 169 pp.